Laser stabilized to a fiber interferometer with close-to-zero temperature sensitivity

Bo Shi, Irene Barbeito Edreira, Meng Ding, Zitong Feng, Win Indra, Francesco Poletti, Giuseppe Marra, Radan Slavík*

Bo Shi, Irene Barbeito Edreira, Meng Ding, Win Indra, Francesco Poletti, Radan Slavík

Optoelectronics Research Centre, University of Southampton, Southampton, SO17 1BJ, UK

E-mail: meng.ding@soton.ac.uk

Zitong Feng, Giuseppe Marra

National Physical Laboratory, Hampton Road, Teddington, TW11 0LW, UK

Keywords: hollow core fibers, fiber delay line, thermally insensitive interferometer, long-term stability, laser stabilization

Abstract: Ultra-stable laser sources typically achieve long-term frequency stability by locking to a bulky and costly vacuum-operated Fabry–Perot cavity made of ultra-low expansion material such as ultra-low expansion glass (ULE). In this work, we demonstrate that long-term stability can be achieved with a specially designed fiber interferometer operated at zero-temperature-sensitivity crossing point, a feature typically achieved only with cavities made from zero-expansion materials. The ultra-low temperature sensitivity is achieved by using a combination of a hollow-core optical fiber that provides the required delay and a short segment of a standard single-mode fiber that provides temperature compensation. Additionally, we placed the interferometer in an airtight aluminum enclosure to mitigate the effect of environmental pressure fluctuations. A laser locked to this interferometer exhibits ±550 kHz peak-to-peak frequency variation over 100 hours of continuous operation, and a frequency drift below 20 Hz/s. The corresponding Allan deviation reaches $2\times10^{-14}\tau$ (for τ>100 s), rivaling performance of miniature ULE cavities. Compared to previously reported fiber and waveguide-based systems operating in ambient conditions, our approach offers superior long-term frequency stability. Owing to its compactness, low cost, and alignment-free design, this system provides a promising solution for deployable frequency references in applications such as geophysics, field spectroscopy, and space-based sensing.

1. Introduction

Frequency-stable lasers are fundamental tools across a variety of scientific and technological applications, including atomic clocks,[1] gravitational wave detection,[2] and ultra-stable microwave generation.[3] In these applications, laser frequency noise is typically suppressed by locking the laser to a stable frequency reference. State-of-the-art performance is often achieved using bulk optics-based Fabry–Perot cavities placed in ultra-stable environments, involving vacuum systems with multi-layer thermal shielding and vibration isolation, sometimes operating at cryogenic temperatures.[4,5] While these setups deliver exceptional short- and long-term frequency stability, they are bulky, sensitive to alignment, and expensive, thereby limiting their applications outside laboratory environments, such as space-based applications. Although compact and portable stable lasers are generally not expected to reach the level of stability offered by the most complex systems, improving their performance and/or reducing their cost and weight promises to increase the number of applications that could use them. Examples of emerging applications are earthquake detection using data-carrying submarine cables or field-deployed spectroscopy.[6,7]

To bridge the gap between ultimate performance and compactness, significant efforts have been directed towards developing compact and robust laser frequency stabilization systems. Representative approaches include miniature Fabry-Perot (FP) cavities, [8–12] on-chip integrated resonators, [13–15] whispering-gallery-mode (WGM) resonators, [16–18] and optical fiber delay lines[19–22]. Most of these systems have demonstrated fractional instability at 10^{-13} to 10^{-14} level at averaging time below 1 s. For instance, miniature ultra-low expansion (ULE) FP cavities achieved 10^{-14} level at 1 s, [9,12] monolithic FP cavity achieved 10^{-13} at 20 ms, [8] and the integrated coil resonator achieved 5×10^{-14} level at 10 ms.[15] Optical fiber delay lines have shown instabilities as low as 3.2×10^{-15} at 1 s when placed in vacuum[23] and 6.3×10^{-15} at 16 ms in ambient conditions.[19]

Despite the promising short-term performance of all these compact systems, the long-term stability (time scales beyond 1-100 seconds) is usually limited. Apart from ULE-FP cavities, it is often because of relatively large thermo-optic coefficient of the material through which the light propagates. However, stability over long time scales is required in many applications, e.g., earthquake detection and gas spectroscopy.

Thanks to guidance through an empty (or air-filled) core, hollow-core fibers (HCFs)[24] have very low thermo-optic coefficient, especially when compared to single-mode fibers (SMFs), waveguides, or WGM resonators. The variation of optical path length in HCF in response to temperature variations is about 20 times smaller than that of SMF[25], making HCF an interesting alternative to SMF in fiber delay lines. Importantly, we have previously reported several HCF interferometer configurations that further reduce this temperature sensitivity[26–32] , reaching levels comparable to those of miniature ULE-FP cavities. However, despite this promising potential, none of them have been demonstrated so far for laser stabilization or designed and studied for long-term stability.

In this article, we phase lock a laser to one of the HCF delay line configurations that reaches zero thermal sensitivity[28] and study its long-term stability when operated in a non-vacuum environment. To achieve this, we firstly use an improved HCF design that achieves simultaneously optimized thermal stability and mechanical strength.[33] Further, we show that once the interferometer is optimally compensated (i.e., operating near zero-temperature-sensitivity point), it is limited by fibers' pressure sensitivity. We address this by placing them in a sealed box, subsequently achieving laser locking with a frequency variation within a small range of ±550 kHz measured over 100 hours of continuous operation. The corresponding frequency drift was below 20 Hz/s and frequency instability of 10^{-11} over 1 000 s. This represents, to the best of our knowledge, the best stability of a non-vacuum reference fiber or waveguide system operating over such long time scales. Thanks to its compactness and alignment-free nature, it is expected to be of interest in a range of applications requiring a low-cost, compact, and field-deployable optical reference.

2. Compensated fiber interferometer: set-up

The principle of the thermally insensitive fiber delay line interferometer studied here was introduced in [28] and is illustrated in **Figure 1**a. We refer to it as 'Compensated interferometer'. It consists of an interferometer in which one arm is formed by a long length of an HCF while the other arm is formed by a short segment of SMF. Temperature insensitivity is then achieved through control of the HCF and SMF lengths, as illustrated below.

In our implementation, the HCF segment is 52 m long. Given HCF's phase thermal sensitivity of 1.6 rad/m/ºC (0.4 ppm/ºC)[26], light propagating through the HCF segment changes its phase with temperature at the rate of 83.2 rad/ºC. The same phase change rate is achieved in thinly

coated SMF as short as about 2.6 m, as its phase thermal sensitivity was measured to be 32 rad/m/°C (5.44 ppm/°C) and therefore significantly higher than that of the HCF. Consequently, a change in ambient temperature induces the same phase changes in both interferometer arms, producing no change in the interference observed at the interferometer output, resulting in a temperature-insensitive interferometer response.

As for the HCF, we used an in-house fabricated nested antiresonant nodeless fiber (NANF) that was optimized for thermally-sensitive applications.[33] It has a relatively thick glass diameter (300 µm) and thin acrylate coating (20 µm thickness). It is an improved design over that used previously in the compensated interferometer,[28] with improved thermal response and mechanical stability. The SMF is also fabricated in-house, with standard 125 µm glass diameter, but single-layer coating thickness of only 30 µm. We have previously shown that this coating can strongly suppress the effects of fiber optical length relaxation due to the typical acrylate coating viscoelastic properties.[26]

The structure of the compensated fiber interferometer is shown in **Figure 1**b. HCF is spliced in between the 80% output port of a 20:80 optical coupler and one input port of a 3×3 coupler used for unambiguous phase extraction.[26] Stronger signal sent through the HCF interferometer arm via the 20:80 coupler compensated for larger loss in that arm, caused mainly by the two SMF-HCF interfaces (about 1.5 dB each) and the HCF loss. The SMF-HCF splice used a graded-index (GRIN) bridge fiber of ¼ pitch length[34] to accommodate for different mode field diameter (MFD) of the SMF (10.4 µm) and the used HCF (24 µm). The fibers of both arms were wound onto the same 10-cm diameter spool. Winding both fibers together should minimize the temperature difference experienced between the two fibers. Two thermistors were installed to monitor the temperature – one directly onto the fibers and one in the middle of the fiber spool, **Figure 2**d.

Subsequently, the compensated interferometer was enclosed in an air-tight aluminum box fitted with in-house made wire and fiber feed-throughs, which were sealed using epoxy as shown in **Figure 1**c. This air-tight aluminum box was then placed inside a thermal chamber capable of stabilizing the internal temperature with accuracy of ±10 mK using a Laird PR-59 temperature controller.

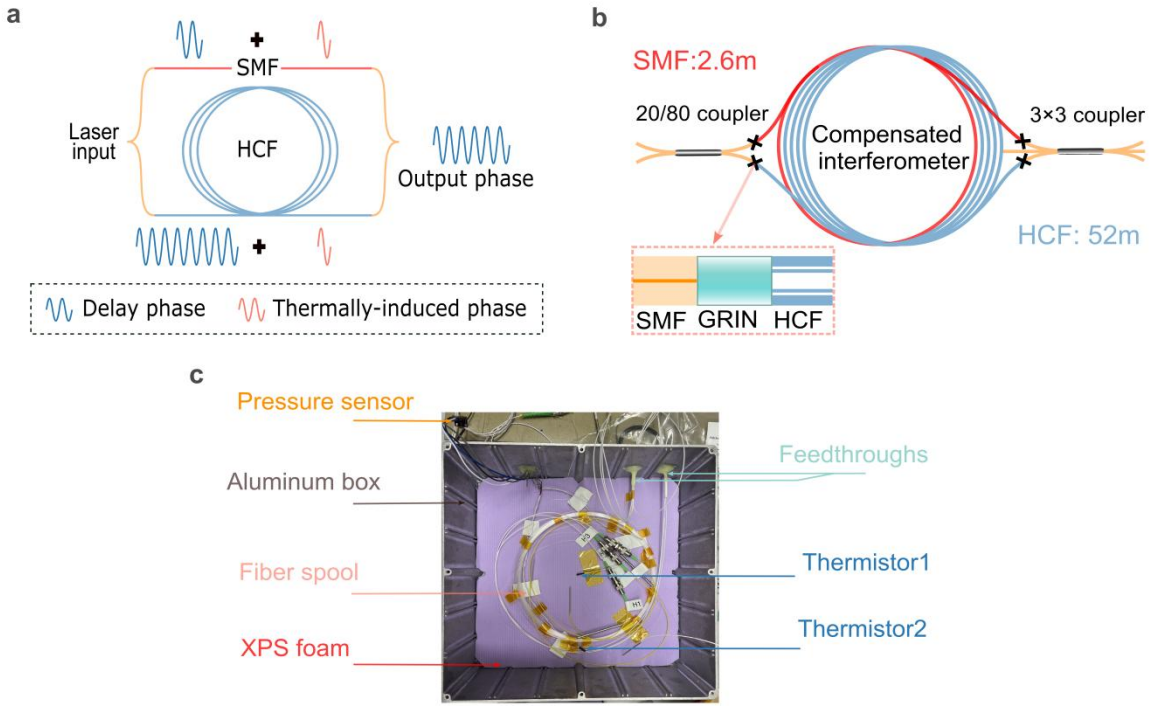

Figure 1. Thermally insensitive compensated fiber interferometer. a) Schematic of the compensated fiber delay line interferometer using HCF and SMF as two fibers with significantly different phase thermal sensitivities. Their length ratio is chosen such that any temperature-induced phase difference is the same in both arms and thus cancels out at the interferometer output. b) Schematics of the experimentally realized compensated interferometer with SMF and HCF wound together with 20/80 input coupler and 3x3 output coupler. Inset: spliced mode-field adaptation between the SMF and HCF using a ¼-ptich segment of GRIN fiber. c) Photograph of the interferometer set-up, placed in aluminum box with thermistors and in-house-made pressure-tight feed throughs for fibers and wires.

3. Response to temperature

The response of the compensated interferometer was measured using the experimental setup shown in **Figure 2**a. As the probe light source, we used narrow linewidth laser emitting at 1558 nm (RIO from Luna Inc.). To ensure that the measured output is attributable to the change in the interferometer rather than to the frequency drift of the laser, we phase locked the probe laser to a carrier-envelope offset (CEO) stabilized optical frequency comb (OFC). The three output signals from the 3×3 coupler were monitored with three photodetectors. The signals from the photodetectors were recorded and interferometer phase change was subsequently extracted using the procedure described in [35].

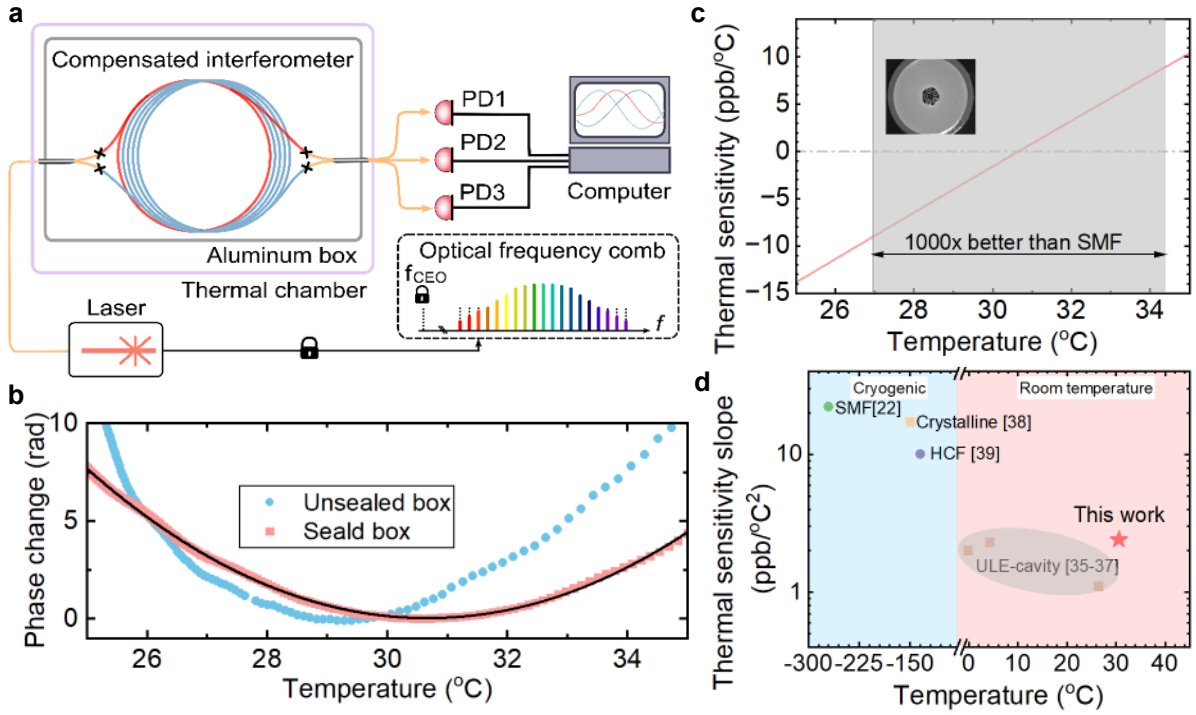

Figure 2. Characterization of thermal sensitivity of the compensated interferometer. a) Measurement set-up. b) Measured phase change at the interferometer output when temperature was changed from 25 to 35 °C. c) Thermal sensitivity calculated from the sealed box data shown in (b), showing thermal sensitivity crossing zero at 30.7 °C with the slope of 2.4 ppb/°C^2. This small slope makes the interferometer 1 000 times less thermally sensitive than SMF-made interferometer over temperature range of 7 °C (grey area). d) Comparison of zero thermal sensitivity crossing temperatures and thermal sensitivity slopes for various optical reference technologies that were reported to show zero-sensitivity crossing.

Firstly, we evaluated thermal sensitivity of the interferometer by characterizing its response to temperature. **Figure 2**b shows how the interferometer phase changes with the thermal chamber temperature, which varies from 25 to 35 °C. As we discuss later, we subsequently eliminated influence of the ambient pressure variations by sealing the aluminium box. Thus, in **Figure 2**b, we show results of two measurements: with the box open (i.e., at approximately constant pressure) and with the box sealed (at approximately constant volume). Compared with the open-box condition, the sealed configuration exhibits a slight reduction in the thermal induced phase change. It can be explained considering the ideal gas law, which predicts $\Delta p/\Delta T = p_0/T_0 \sim 350$ Pa/°C, where p_0 is the air pressure and T_0 is the average temperature of the box. Given the HCF's pressure sensitivity (discussed in the next section) of -1.5×10^{-11}/Pa, the temperature-induced pressure variation causes an additional phase change of about -5×10^{-9}/°C. This effect slightly reduces the constant-volume thermal sensitivity by roughly 5 ppb/°C compared with the constant-pressure case, leading to about 1 °C increase in the zero-crossing temperature. As the interferometer will be used in a sealed configuration for the subsequent laser-locking

experiments, we consider only the thermal sensitivity measured in the sealed box (at constant volume) throughout the rest of the paper.

Figure 2b shows that phase change with temperature closely follows a quadratic polynomial. Its derivative then gives the thermal sensitivity, which is shown in **Figure 2**c after normalization to accumulated phase in the interferometer (in ppb/°C). It crosses zero at 30.7 °C. It is worth mentioning that by slightly adjusting the length of the SMF, the zero-crossing temperature the compensated interferometer can be increased or decreased, as discussed in Ref. [28]. In our experiment, when the SMF length was changed by 15 cm (from 2.55 m to 2.70 m), the zero-crossing temperature shifted by ~0.8 °C, corresponding to a slope of 0.2°C/cm. Considering SMF length control within ±0.5 cm, the zero-crossing temperature can be set with an accuracy of approximately ±0.1 °C. Compared to thermal sensitivity of the HCF used in this study (which was measured to be 0.4 ppm/°C), the compensated interferometer has 40-times lower sensitivity over 8 °C (26.5 – 34.8 °C, 10 ppb/°C) temperature range. When compared to an SMF fiber interferometer (sensitivity of 8 ppm/°C), this represents an improvement over 1 000 times over 7 °C temperature range. Keeping the interferometer within such temperature range can be achieved with simple temperature control and with only basic thermal shielding, without vacuum, representing significant simplification, reduction on the size, weight and cost and thus significantly improving its ability to be deployed in the field.

Figure 2d compares the temperature at which zero-sensitivity was achieved with different optical references and also the thermal sensitivity slopes,[22,36–40] which is relevant to the above-discussed temperature range over which the interferometer can be operated with the desired level of stability.

4. Response to ambient pressure

Once sensitivity to temperature fluctuations has been strongly suppressed by operating the compensated interferometer in the vicinity of its zero-sensitivity point, the stability of the interferometer is expected to be limited by other environmental changes, including atmospheric pressure.[41] This is shown in **Figure 3**, where **Figure 3**a shows pressure variation in our laboratory measured over 3 000 s inside an unsealed aluminum box with a pressure sensor attached to the compensated interferometer. **Figure 3**b shows the phase variation of the compensated interferometer measured at the same time, with the temperature stabilized. For better visualization, **Figure 3**c then show these data with linear drift removed. Ambient pressure

(**Figure 3**a) is strongly correlated with observed phase changes shown in **Figure 3**c, showing how interferometer perturbations are influenced by atmospheric pressure variations. Corresponding pressure sensitivity of the compensated interferometer can then be calculated, obtaining 1.5×10^{-11} Pa^{-1}, which is consistent with values given in the literature.[41]

To reduce pressure variations, optical references are typically put into vacuum environments. However, this adds size, weight, and power (SWaP), which is why we investigated an alternative solution in which we simply sealed the aluminum box with silicone. The pressure variation inside the sealed box over 3 000 s is shown in **Figure 3**d. The observed pressure variations are two orders of magnitude smaller in the sealed box as compared to the unsealed one (**Figure 3**a). The interferometer output in the sealed box is then shown in **Figure 3**e with **Figure 3**f showing the phase variations after removing the linear fit. We see that the phase variation in the sealed box is over 10 times smaller than in unsealed box. We operated the sealed box over the time scale of 6 months and did not observe any degradation in the air-tightness, tested by observing the correlation between the temperature and pressure inside the box.

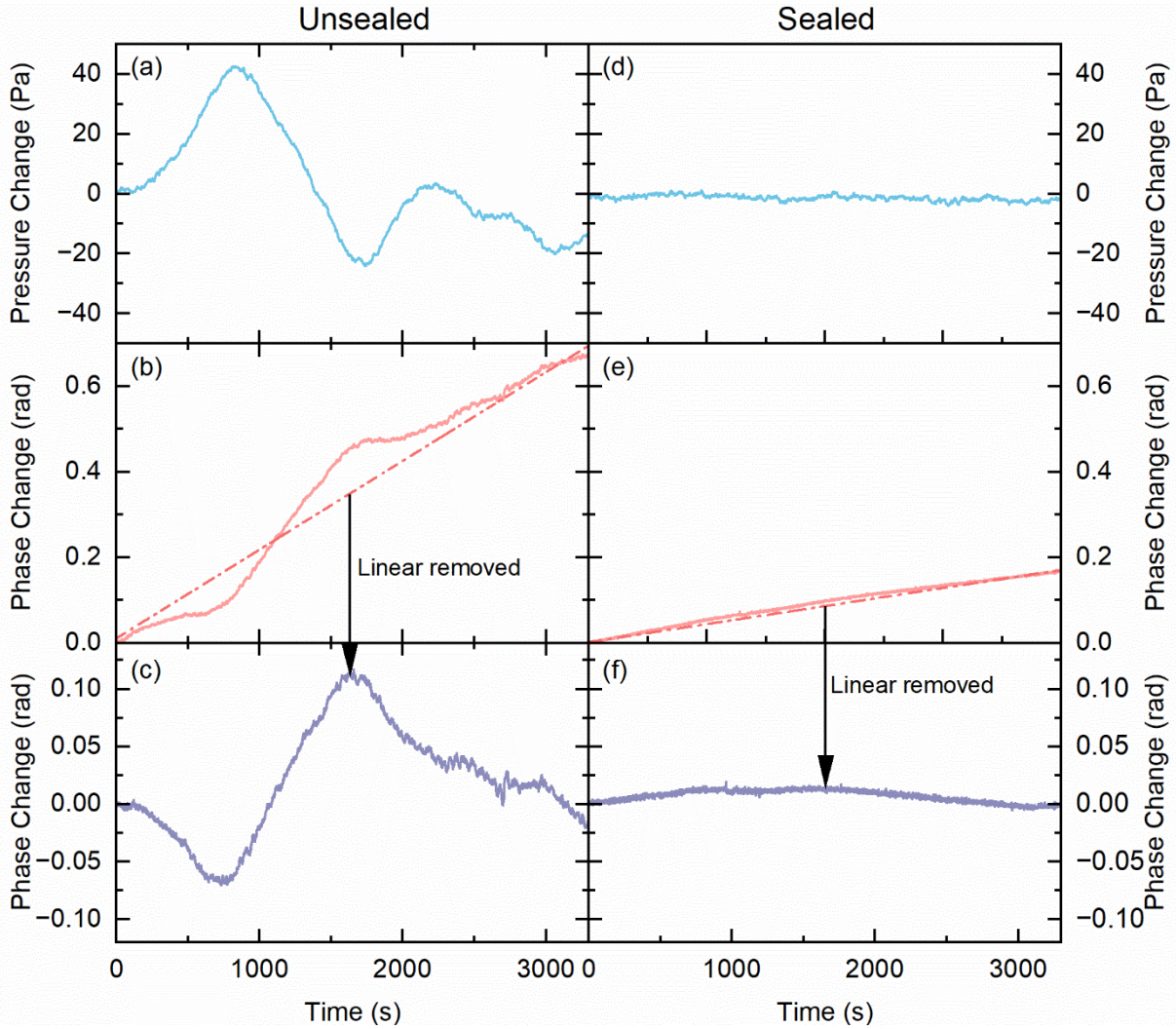

Figure 3. Phase variations before and after sealing the compensated interferometer box. (a,d) Pressure perturbation inside the box before (a) and after (d) sealing over time. (b, e) Measured phase change over the same period before (b) and after (e) sealing. (c, f) Phase change with linear drift removed before (c) and after (f) sealing.

5. Response to temperature variations

Temperature compensation in the compensated interferometer assumes that both interferometer arms experience the same temperature changes. Thus, we have ensured that the temperature experienced by both interferometer arms is as equal as possible, specifically winding the fibers together, putting them in between two insulating sheets, and surrounding them by the aluminum box that has good thermal conductivity. However, temperature gradients experienced in real-world operations may introduce slight differences in temperatures of the two interferometer arms. To gain an insight into the performance under temperature gradients, we sinusoidally modulated the temperature with 1°C amplitude and monitored the phase at the compensated interferometer output. During the temperature cycling, uneven heat propagation within the box

leads to spatially non-uniform temperature changes. Consequently, two arms of the interferometer may experience slightly different temperature variations. The sinusoidal modulation was therefore applied to emulate realistic environmental conditions in which temperature fluctuations are gradual, but not spatially uniform. This enables a more representative assessment of the interferometer's thermal stability and its temperature-insensitive performance under practical operating conditions. We performed this experiment at average temperatures ranging from 29 to 35°C, **Figure 4**. Here, we can observe that the thermal sensitivity of the compensated fiber interferometer changes from clearly negative (phase changes in opposite direction to temperature) at the lowest measured average temperature of 29.6°C to clearly positive (temperature and phase change has the same sign) at the highest measured average temperature of 34.3°C. The smallest phase variation of 0.6 rad (peak-to-peak) was measured for average temperatures of 30.5 and 31.5°C, **Figure 4**. This temperature is consistent with earlier characterization showing zero sensitivity temperature of 30.7 °C. The residual phase variation of 0.6 rad with 1°C temperature variation corresponds to effective phase sensitivity of 3 ppb/°C, which is >100 times less than in HCF-based interferometer and 2500 times less than in an SMF based interferometer.

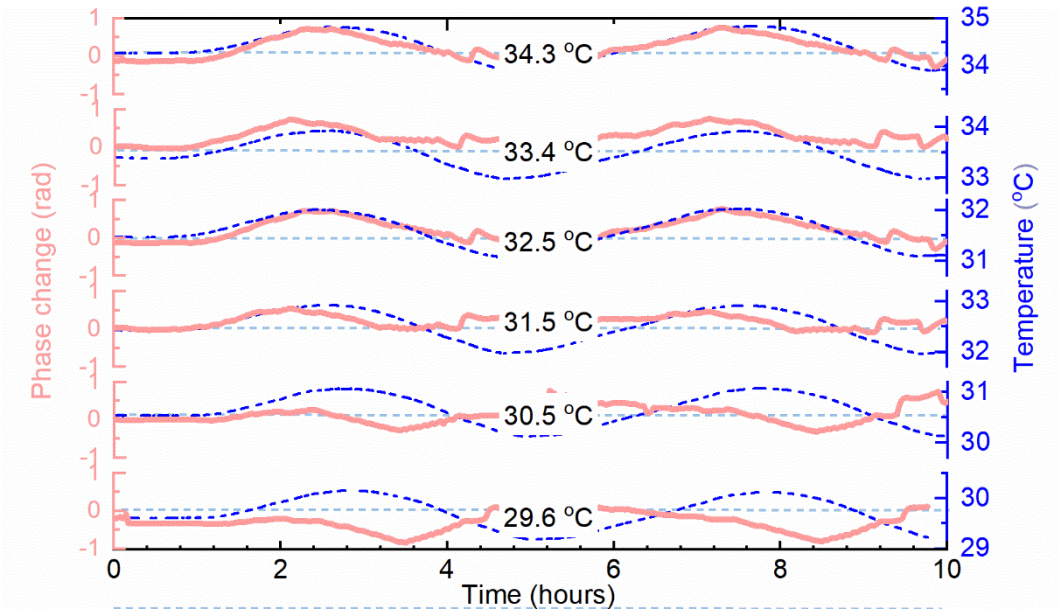

Figure 4. Phase response (red solid) of interferometer inside the sealed aluminum box subject to 1°C temperature modulation (dark blue) for average temperatures of 29.6, 30.5, 31.5, 32.5, 33.4, and 34.3°C.

6. Laser locked to the compensated interferometer

To evaluate performance of a laser locked to the compensated interferometer, the interferometer temperature was first stabilized at the zero-sensitivity temperature. The set-up of laser locking to the compensated interferometer and its stability characterization is shown in **Figure 5**. Laser used for locking was Rock laser (NP Photonics Inc.), 10% of its power was tapped (using a 90/10 coupler) to phase lock it to the compensated interferometer using Moku FPGA board (Liquid Instruments) using Pound-Drever-Hall (PDH) technique. The laser was then combined with signal of the CEO-stabilized optical frequency comb and the photodetected beat was subsequently compared to the comb frequency reference using zero dead time frequency counter (Keysight 53230A) with clock synchronized by the RF signal from the optical frequency comb.

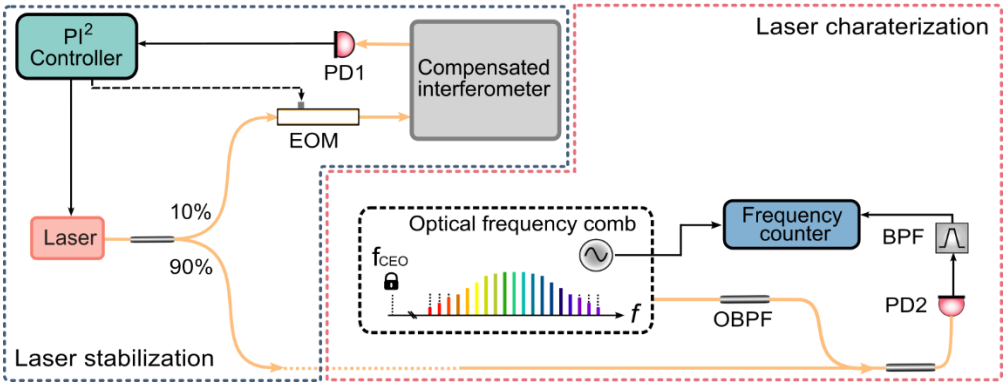

Figure 5. Set up of laser locked to the compensated interferometer and its stability characterization via comparison to the CEO-stabilized optical frequency comb. EOM: Electro-optic modulator, OBPF: Optical bandpass filter, PD: photodetector, BPF: RF bandpass filter.

The beat frequency variation measured with the stabilized laser over 100 hours is shown in **Figure 6**a. The laser stayed locked over the entire period; however, OFC went out of lock between hour 42 and 50, causing a gap in the measured data, **Figure 6**a. The peak-to-peak frequency error stayed within ±550 kHz. The frequency drift calculated by differentiating data from **Figure 6**a is shown in **Figure 6**b and stayed within -18 and 10 Hz/s. The origin of this frequency drift is likely complex, and its underlying physical mechanisms are yet to be fully studied. We also calculated the Allan deviation from the laser frequency variation (**Figure 6**a), which is shown in **Figure 6**c. Allan deviation shows a linear trend with averaging time τ and follows $\approx 2\times10^{-14}\ \tau$ for $\tau > 100$ s. For $\tau < 100$ s, the performance is likely ~~to be~~ limited by vibration and acoustic pick up. Although we expect this could be further improved, e.g., by using acoustic and vibration insensitive fiber spools [21], no particular attention was given to this here, as the focus of this work was on characterizing long-term stability. Compared to the

performance of the free-running Rock laser and other commercially available lasers (also shown in **Figure 6**b), our compensated interferometer locked laser shows 2 orders of magnitude lower Allan deviation.

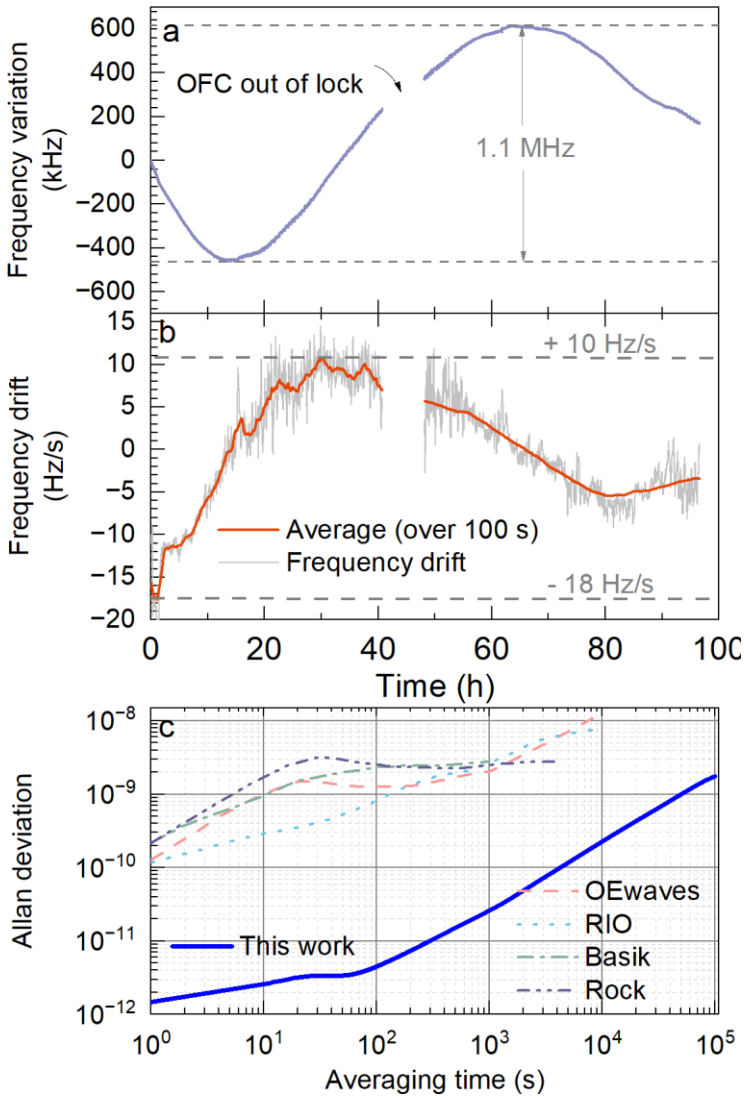

Figure 6. Characterization of laser stabilized to the compensated interferometer. a) The frequency variation of the laser stabilized by the compensated fiber interferometer over almost 100 hours. b) Frequency drift calculated from data shown in a), showing slope within ±20 Hz/s. c) Allan deviation calculated from data shown in a) and its comparison to free-running laser, and other three commercially available lasers.[42]

7. Discussion/Conclusion

7.1 Discussion

To evaluate the performance of our compensated interferometer-stabilized laser, we compare it with performance of lasers stabilized to other compact optical reference systems designed to operate without vacuum and thus target field-deployable solution, **Table 1**. The Q factor, Q =

ν/δν (carrier frequency ν = 193.5 THz at 1550 nm, the resonance linewidth full width at half-maximum δν) was evaluated as follows. In the used Mach-Zehnder interferometer configuration, δν equals half of the interference period. This interference period is $c/(\delta L)$, where c is the speed of the light, and $\delta L = L_{HCF}\text{-}n\times L_{SMF}$ is the optical length difference between the two arms. The Q factor, computed using $\delta\nu = c/(2\delta L)$ was then 6.2×10^7.

Table 1 Comparison of various configurations of lasers locked to an optical reference that was not placed in vacuum.

Optical reference	Q factor	Frequency drift (Hz/s)	Allan deviation reported up to (s)	Allan deviation slope (s^{-1})
On chip Si_3N_4 coil[15]	1.4×10^8	2300	4	1.2×10^{-11}
MgF_2 WGM[43]	2×10^9	38	1000	1.2×10^{-13}
WGMR[17]	6×10^8	Unknown	500	1.5×10^{-12}
Monolithic silica FP[8]	6.4×10^8	100-1000	100	1.5×10^{-12}
μ-ULE FP[9]	1.2×10^{10}	2.8	10	1×10^{-14}
Vacuum-gap ULE FP[12]	4.8×10^9	5	100	2×10^{-14}
SMF delay line[21]	4.5×10^9	270	10	2×10^{-12}
SMF delay line[19]	4×10^9	28-270	10	2×10^{-13}
HCF-FP[42]	4.2×10^9	< 70	100 000	2×10^{-13}
This work	**6.2×10^7**	**< 20**	**100 000**	**2×10^{-14}**

All these stabilized lasers show a linear increase of Allan deviation with averaging time τ beyond certain τ, meaning that at long time scale, they all behave as $s(\tau)=a\cdot\tau$ with the Allan deviation slope a shown in **Table 1**. As shown here, our system shows one of the best Allan deviation slopes, with comparable performance to cavities made of ultra-low expansion (ULE) glass, which are also insensitive to temperature variations. Notably, our system outperforms all other fiber-based systems, including SMF delay-line (by two orders of magnitud) as well as HCF-made FP reference (by one order of magnitud) in frequency stability at long term scale, despite being operated with low-performance (±10 mK) temperature control. Given that the achieved performance was obtained without vacuum and with a simple temperature controller, it represents a low cost and low power solution suitable for field applications. These characteristics make it particularly suitable for fiber-based sensing, long-haul interferometry,

and cost-sensitive laser stabilization applications (e.g., geophysics, field spectroscopy, RF photonics).

Although our HCF sample was coiled with coil radius of 7 cm, HCFs that are bend-insensitive down to radii below 5 mm have been reported [44], which would allow here-used HCF length of 52 m to be coiled to a coil with radius of 15 mm and height of 10 mm, potentially enabling compact, field -deployable solution.

Compared to integrated optics solutions, HCF should allow for lower fundamental noises such as thermo-conductive noise [15] due to strong suppression of light-glass interaction in the light path. Additionally, the extremely low thermal sensitivity of the compensated interferometer (>1000 times lower than in SMF or integrated optics light guiding materials) should result in significantly better long-term performance. Integrated optics typically provide advantages in cost and size; however, our configuration is expected to be of particular interest when higher performance is needed than integrated-optics solutions can deliver.

We also hypothesize that the current limitations such as residual phase fluctuations may be caused by polarization mode dispersion (PMD), which could be addressed in future by adopting a Michelson interferometer configuration with Faraday rotator mirrors, as demonstrated in prior work [19].

7.2 Conclusion

This paper presents a compensated fiber delay-line interferometer with significantly improved thermal stability. By employing HCF with lower thermal sensitivity in the long delay arm and a short segment of SMF with higher thermal sensitivity in another arm, thermally induced phase shift is strongly suppressed. Firstly, we showed that the interferometer's output phase is thermally insensitive, with thermal sensitivity crossing zero at temperature of 30.8°C. Once the effect of temperature is minimized, we show that the system is limited by environmental pressure variations. We addressed this by placing the interferometer into a sealed enclosure.
Subsequently, we measured frequency stability of a laser locked to the compensated interferometer over an extended period of 100 hours, demonstrating its robustness. During this time, the maximum variation in the frequency variation was below ±550 kHz, with frequency drifting below 20 Hz/s. This is at similar performance level as achieved in miniature ULE cavities, however, without any free space alignment. The achieved frequency drift is also at

least an order of magnitude lower than for any other fiber or integrated optics system operated in non-vacuum environments. Consequently, our compensated hollow core fiber system fills the performance/cost/practicality gap between laboratory-based systems (such as those based on vacuum-placed ULE-cavities) and other field-deployable solutions. It is of interest to a range of applications such as seismic sensing using installed fiber cables, pure RF generation, gas sensing[45–47] and space missions such as gravity mapping and climate observation.

Acknowledgements

This work was financially supported by the UK Engineering and Physical Sciences Research Council (EP/W037440/1), European Research Council (682724), and UK Royal Academy of Engineering. Further, it has been supported by UK Department for Science Innovation and Technology through the National Measurement System Program.

Conflict of Interest

The authors declare no conflicts of interest.

Data Availability Statement

The data that support the findings of this study are available through the University of Southampton research repository via DOI: 10.5258/SOTON/XXXX.

Received: ((will be filled in by the editorial staff))
Revised: ((will be filled in by the editorial staff))
Published online: ((will be filled in by the editorial staff))

References

[1] Y. Y. Jiang, A. D. Ludlow, N. D. Lemke, R. W. Fox, J. A. Sherman, L.-S. Ma, C. W. Oates, *Nat. Photonics* **2011**, *5*, 158.
[2] B. P. Abbott, R. Abbott, R. Adhikari, et.al., *Reports Prog. Phys.* **2009**, *72*, 076901.
[3] I. Kudelin, P. Shirmohammadi, W. Groman, S. Hanifi, M. L. Kelleher, D. Lee, T. Nakamura, C. A. McLemore, A. Lind, D. Meyer, J. Bai, J. C. Campbell, S. M. Bowers, F. Quinlan, S. A. Diddams, *Nat. Electron.* **2024**, *7*, 1170.
[4] D. Kedar, J. Yu, E. Oelker, A. Staron, W. R. Milner, J. M. Robinson, T. Legero, F. Riehle, U. Sterr, J. Ye, *Optica* **2023**, *10*, 464.
[5] D. Kedar, Z. Yao, I. Ryger, J. L. Hall, J. Ye, *Optica* **2024**, *11*, 58.
[6] S. Coburn, C. B. Alden, R. Wright, K. Cossel, E. Baumann, G.-W. Truong, F. Giorgetta, C. Sweeney, N. R. Newbury, K. Prasad, I. Coddington, G. B. Rieker, *Optica* **2018**, *5*, 320.
[7] G. Marra, C. Clivati, R. Luckett, A. Tampellini, J. Kronjäger, L. Wright, A. Mura, F.

Levi, S. Robinson, A. Xuereb, B. Baptie, D. Calonico, *Science* **2018**, *361*, 486.
[8] W. Zhang, L. Stern, D. Carlson, D. Bopp, Z. Newman, S. Kang, J. Kitching, S. B. Papp, *Laser Photon. Rev.* **2020**, *14*.
[9] J. Guo, C. A. McLemore, C. Xiang, D. Lee, L. Wu, W. Jin, M. Kelleher, N. Jin, D. Mason, L. Chang, A. Feshali, M. Paniccia, P. T. Rakich, K. J. Vahala, S. A. Diddams, F. Quinlan, J. E. Bowers, *Sci. Adv.* **2022**, *8*.
[10] W. Liang, Y. Liu, *Opt. Lett.* **2023**, *48*, 1323.
[11] C. A. McLemore, N. Jin, M. L. Kelleher, Y. Luo, D. Lee, Y. Liu, T. Nakamura, D. Mason, P. Rakich, S. A. Diddams, F. Quinlan, *Opt. Lett.* **2024**, *49*, 4737.
[12] Y. Liu, N. Jin, D. Lee, C. McLemore, T. Nakamura, M. Kelleher, H. Cheng, S. Schima, N. Hoghooghi, S. Diddams, P. Rakich, F. Quinlan, *Optica* **2024**, *11*, 1205.
[13] W. Jin, Q. F. Yang, L. Chang, B. Shen, H. Wang, M. A. Leal, L. Wu, M. Gao, A. Feshali, M. Paniccia, K. J. Vahala, J. E. Bowers, *Nat. Photonics* **2021**, *15*, 346.
[14] A. Isichenko, A. S. Hunter, D. Bose, N. Chauhan, M. Song, K. Liu, M. W. Harrington, D. J. Blumenthal, *Sci. Rep.* **2024**, *14*, 27015.
[15] K. Liu, N. Chauhan, J. Wang, A. Isichenko, G. M. Brodnik, P. A. Morton, R. O. Behunin, S. B. Papp, D. J. Blumenthal, *Optica* **2022**, *9*, 770.
[16] A. E. Shitikov, I. A. Bilenko, N. M. Kondratiev, V. E. Lobanov, A. Markosyan, M. L. Gorodetsky, *Optica* **2018**, *5*, 1525.
[17] W. Liang, V. S. Ilchenko, D. Eliyahu, A. A. Savchenkov, A. B. Matsko, D. Seidel, L. Maleki, *Nat. Commun.* **2015**, *6*, DOI 10.1038/ncomms8371.
[18] L. M. Baumgartel, R. J. Thompson, N. Yu, *Opt. Express* **2012**, *20*, 29798.
[19] I. Jeon, W. Jeong, C. Ahn, J. Kim, *Opt. Lett.* **2025**, *50*, 1057.
[20] I. B. Edreira, R. Slavík, J. K. Sahu, M. Núñez-Velázquez, L. Wright, M. Schioppo, G. Marra, *Opt. Express* **2024**, *32*, 16823.
[21] I. Jeon, C. Ahn, C. Kim, S. Park, W. Jeon, L. Duan, J. Kim, *APL Photonics* **2023**, *8*, DOI 10.1063/5.0160834.
[22] B. Merkel, D. Repp, A. Reiserer, *Opt. Lett.* **2021**, *46*, 444.
[23] Y. Huang, D. Hu, M. Ye, Y. Wang, Y. Li, M. Li, Y. Chen, Q. Qu, L. Wang, L. Liu, T. Li, *Chinese Opt. Lett.* **2023**, *21*, 031404.
[24] Y. Chen, M. N. Petrovich, E. N. Fokoua, A. I. Adamu, M. R. A. Hassan, H. Sakr, R. Slavík, S. B. Gorajoobi, M. Alonso, R. F. Ando, A. Papadimopoulos, T. Varghese, D. Wu, M. F. Ando, K. Wisniowski, S. R. Sandoghchi, G. T. Jasion, D. J. Richardson, F. Poletti, in *Opt. Fiber Commun. Conf. 2024*, Optica Publishing Group, Washington, D.C., **2024**, p. Th4A.8.
[25] R. Slavík, G. Marra, E. N. Fokoua, N. Baddela, N. V. Wheeler, M. Petrovich, F. Poletti, D. J. Richardson, *Sci. Rep.* **2015**, *5*, 15447.
[26] B. Shi, H. Sakr, J. Hayes, X. Wei, E. Numkam Fokoua, M. Ding, Z. Feng, G. Marra, F. Poletti, D. J. Richardson, R. Slavík, *Opt. Lett.* **2021**, *46*, 5177.
[27] R. Slavík, E. R. Numkam Fokoua, M. Bukshtab, Y. Chen, T. D. Bradley, S. R. Sandoghchi, M. N. Petrovich, F. Poletti, D. J. Richardson, *Opt. Lett.* **2019**, *44*, 4367.
[28] B. Shi, G. Marra, Z. Feng, H. Sakr, J. R. Hayes, E. R. N. Fokoua, M. Ding, F. Poletti, D. J. Richardson, R. Slavik, *J. Light. Technol.* **2022**, *40*, 5716.
[29] M. Ding, E. N. Fokoua, J. R. Hayes, H. Sakr, P. Horak, F. Poletti, D. J. Richardson, R. Slavík, *Opt. Lett.* **2022**, *47*, 2510.
[30] I. B. Edreira, M. Ding, B. Shi, Z. Feng, G. Marra, I. A. Davidson, J. Rzegocki, S. M. A. Mousavi, G. T. Jasion, F. Poletti, R. Slavík, in *2023 IEEE Photonics Conf.*, IEEE, **2023**, pp. 1–2.
[31] X. Wei, A. Taranta, B. Shi, M. Ding, Z. Feng, D. J. Richardson, F. Poletti, R. Slavík, *J. Light. Technol.* **2023**, *41*, 3145.

[32] M. Ding, I. A. Davidson, G. Jasion, B. Shi, J. R. Hayes, P. C. Schultz, D. J. Richardson, F. Poletti, R. Slavík, *Sci. Adv.* **2025**, *11*, eads7529.
[33] B. Shi, I. A. Davidson, G. A. Mahdiraji, J. Rzegocki, E. R. Numkam Fokoua, M. Mousavi, Z. Feng, M. Ding, F. Poletti, D. J. Richardson, R. Slavík, in *2023 Jt. Conf. Eur. Freq. Time Forum IEEE Int. Freq. Control Symp.*, IEEE, **2023**, pp. 1–2.
[34] M. Komanec, D. Suslov, S. Zvánovec, Y. Chen, T. Bradley, S. R. Sandoghchi, E. R. N. Fokoua, G. T. Jasion, M. N. Petrovich, F. Poletti, D. J. Richardson, R. Slavík, *IEEE Photonics Technol. Lett.* **2019**, *31*, 723.
[35] K. P. Koo, A. B. Tveten, A. Dandridge, *Appl. Phys. Lett.* **1982**, *41*, 616.
[36] S. Häfner, S. Falke, C. Grebing, S. Vogt, T. Legero, M. Merimaa, C. Lisdat, U. Sterr, *Opt. Lett.* **2015**, *40*, 2112.
[37] I. Ito, A. Silva, T. Nakamura, Y. Kobayashi, *Opt. Express* **2017**, *25*, 26020.
[38] Z. Wang, Y. Ye, J. Chang, J. Zhang, Y. Sun, L. He, Q. Wu, Z. Lu, J. Zhang, *Opt. Express* **2021**, *29*, 30567.
[39] T. Kessler, C. Hagemann, C. Grebing, T. Legero, U. Sterr, F. Riehle, M. J. Martin, L. Chen, J. Ye, *Nat. Photonics* **2012**, *6*, 687.
[40] Z. Feng, H. Sakr, J. R. Hayes, E. N. Fokoua, M. Ding, F. Poletti, D. J. Richardson, R. Slavík, *Opt. Lett.* **2023**, *48*, 763.
[41] M. Pang, W. Jin, *Opt. Express* **2009**, *17*, 11088.
[42] Z. Feng, M. Ding, M. Komanec, S. Zvánovec, A. Zhong, F. Poletti, G. Marra, R. Slavík, *Photonics Res.* **2025**, *13*, 611.
[43] J. Alnis, A. Schliesser, C. Y. Wang, J. Hofer, T. J. Kippenberg, T. W. Hänsch, *Phys. Rev. A* **2011**, *84*, 011804.
[44] Ghafour Amouzad Mahdiraji, Gregory Jackson, M. R. Naveen Krishna Baddela, Jaroslaw Rzegocki, Gianluca Guerra, and F. P. Chiang Ping Saw, Ian A. Davidson, Gregory T. Jasion, Austin Taranta, in *51th Eur. Conf. Opt. Commun. (ECOC 2025)*, **2025**, p. Th.03.01.2.
[45] Z. Wang, Q. Nie, H. Sun, Q. Wang, S. Borri, P. De Natale, W. Ren, *Light Sci. Appl.* **2024**, *13*, 11.
[46] H. Sun, M. Hu, Q. Nie, Z. Wang, C. Wei, W. Ren, *Appl. Phys. Lett.* **2024**, *125*, DOI 10.1063/5.0242523.
[47] Q. Nie, G. Lyu, C. Wei, W. Ren, *Laser Photon. Rev.* **2025**.